A Heterodimerizing Leucine Zipper Coiled Coil System for Examining the Specificity of **a** Position Interactions: Amino Acids I, V, L, N, A, and K

Asha Acharya,[‡] Sergei B. Ruvinov,[§] Jozsef Gal,[‡] Jonathan R. Moll,[‡] and Charles Vinson*[,‡]

Laboratory of Metabolism and Laboratory of Biochemistry, National Cancer Institute, National Institutes of Health, Bethesda, Maryland 20892

Received July 22, 2002

ABSTRACT: We use a heterodimerizing leucine zipper system to examine the contribution of the interhelical **a**−**a′** interaction to dimer stability for six amino acids (A, V, L, I, K, and N). Circular dichroism (CD) spectroscopy monitored the thermal denaturation of 36 heterodimers that generate six homotypic and 30 heterotypic **a**−**a′** interactions. Isoleucine (I−I) is the most stable homotypic **a**−**a′** interaction, being 9.2 kcal/mol per dimer more stable than the A−A interaction and 4.0 kcal/mol per dimer more stable than either the L−L or V−V interaction, and 7.0 kcal/mol per dimer more stable than the N−N interaction. Only lysine was less stable than alanine. An alanine-based double-mutant thermodynamic cycle calculated coupling energies between the **a** and **a′** positions in the heterodimer. The aliphatic amino acids L, V, and I prefer to form homotypic interactions with coupling energies of −0.6 to −0.9 kcal/mol per dimer, but the heterotypic aliphatic interactions have positive coupling energies of <1.0 kcal/mol per dimer. The asparagine homotypic interaction has a coupling energy of −0.5 kcal/mol per dimer, while heterotypic interactions with the aliphatic amino acids produce coupling energies ranging from 2.6 to 4.9 kcal/mol per dimer. The homotypic K−K interaction is 2.9 kcal/mol per dimer less stable than the A−A interaction, but the coupling energy is only 0.3 kcal/mol per dimer. Heterotypic interactions with lysine and either asparagine or aliphatic amino acids produce similar coupling energies ranging from −0.2 to −0.7 kcal/mol per dimer. Thus, of the amino acids that were examined, asparagine contributes the most to dimerization specificity because of the large positive coupling energies in heterotypic interactions with the aliphatic amino acids which results in the N−N homotypic interaction.

The variable-length leucine zipper coiled coil is the dimerization domain (*1*) of the B-ZIP class of sequence specific transcription factors (*2*−*6*). X-ray crystal studies have demonstrated that the leucine zipper is a dimeric parallel coiled coil (*7*, *8*) that structurally repeats itself every two α-helical turns or every heptad (seven amino acids). Amino acid positions in each heptad are identified using the nomenclature (**a**,**b**,**c**,**d**,**e**,**f**,**g**)$_n$ (*9*).

The **a** and **d** residues are typically hydrophobic and pack in a regular "knobs and holes" pattern (*10*) along the dimerization interface to create the hydrophobic core that contributes most of the energy to leucine zipper dimerization stability (*11*). The **a** position is more variable than the **d** position, and the interhelical interaction between the **a** position and the **a′** position to create the **a**−**a′** interaction may thus contribute to dimerization specificity (*12*). The **a** side chain (knob) packs into the space (hole) created by the four surrounding amino acid side chains, two **d** position side chains on the same α-helix and the **a′** and **g′** side chains on the opposite α-helix of the dimer (*3*). Analysis of coiled coil proteins, found primarily in the structural proteins of the cell, indicates that a variety of hydrophobic amino acids can occupy the **a** position (*13*, *14*). However, the shorter leucine zipper coiled coils found as the dimerization domain of B-ZIP proteins contain a smaller set of amino acids in the **a** position (*12*). The shorter leucine zippers have less protein sequence flexibility because amino acids must be optimized for dimerization stability. Longer leucine zippers, in contrast, allow more regulation of dimerization specificity because they can contain amino acids that are suboptimal for stability but favor interaction with a particular partner.

Determining the contribution of amino acids in the **a** position to dimer stability has been complicated because changing the amino acids in this position can change the oligomerization properties. The leucine zippers of B-ZIP proteins typically contain an asparagine in the **a** position of the second heptad. Changing this asparagine to valine or leucine in the yeast GCN4 B-ZIP protein dramatically stabilizes the structure, but a mixture of dimers and trimers is formed (*15*, *16*). Changing the asparagine to glutamine also resulted in a mixture of dimers and trimers (*17*).

The contribution of amino acids in the homotypic **a**−**a′** interaction to dimer stability has been systematically examined using a covalently closed model coiled coil system (*18*, *19*). This model coiled coil system indicates that the contribution of the aliphatic amino acids to stability is similar to their transfer free energy. A study using a yeast interaction system based on the GCN4 leucine zipper found that interaction between asparagine and isoleucine is disfavored (*20*). Subsequent quantitative work with this system dem-

* To whom correspondence should be addressed. Telephone: (301) 496-8753. Fax: (301) 496-8419. E-mail: Vinsonc@dc37a.nci.nih.gov.
[‡] Laboratory of Metabolism.
[§] Laboratory of Biochemistry.

10.1021/bi020486r
Published on Web 11/09/2002

onstrated that the homotypic I−I interaction is more stabilizing than the N−N interaction (*21*).

We have used a heterodimerizing leucine zipper system to examine the contribution of six amino acids (A, V, I, L, N, and K) in homotypic and heterotypic **a**−**a′** interactions to coiled coil stability. Using an alanine-based double-mutant thermodynamic cycle, we have measured the coupling energy between amino acids in the **a** and **a′** positions to gain insight into amino acid interactions that regulate dimerization specificity. Mixtures of 12 proteins, six mutants for each of the two heterodimerizing proteins, give 36 heterodimers, six homotypic amino acid interactions and 30 heterotypic amino acid interactions in the **a**−**a′** position.

EXPERIMENTAL PROCEDURES

Proteins. The heterodimerizing proteins, derived from the PAR family member VBP B-ZIP domain, are termed B-EE_{34}-(X) and A-RR_{34}(X). The amino acid sequence of the 96-amino acid B-EE_{34}(X) protein is ASMTGGQQMGRDPLEEK-VFVPDEQKDEKYWTRRKKNNVAAKRSRDARRLKEN-QITIRAAFLEKENTALRT**EX**AEL**E**K**E**VGRC**E**NIVSKY-ETRYGPL. The leucine zipper region has been grouped into heptads (**gabcdef**). B represents the basic region, EE_{34} the leucine zipper with the third and fourth **g** ↔ **e′** interaction containing repulsive E ↔ E interactions, and (X) the guest−host position amino acid in the third **a** position. The first 16 amino acids are from the ϕ10 leader sequence and cloning linker, and the 80 remaining amino acids are the B-ZIP domain of VBP with two arginines changed to glutamic acid to create repulsive E ↔ E interhelical interactions (*22*, *23*). The four glutamic acids that produce two repulsive E ↔ E pairs in the third and fourth heptads are bold. The heterodimerizing partner of B-EE_{34}(X) is A-RR_{34}(X), the amino acid sequence of which is ASMTGGQQMGRDP-LEE-LEQ-RAEELARENEELEKEAEELEQENAELEIRAAFLEKEN-TALRT**RX**AEL**R**K**R**VGRC**R**NIVSKYETRYGPL. A represents the acidic extension that can form a coiled coil heterodimeric structure with the VBP basic region (*24*), RR_{34} the leucine zipper with the third and fourth **g** ↔ **e′** interactions containing repulsive R ↔ R interactions, and (X) the guest−host position amino acid in the third **a** position. The four arginines that produce repulsive R ↔ R pairs in the third and fourth heptads are bold.

Protein Purification. Proteins were expressed in *Escherichia coli* BL21 lysE cells using the T7 IPTG-inducible system (*25*). The B-EE_{34}(X) and A-RR_{34}(X) proteins were purified as described previously (*26*). Briefly, the cells were harvested, lysed in low salt after freezing, brought to 1 M KCl, and spun, and the supernatant was dialyzed to low salt. B-EE_{34}(X) proteins that contain DNA binding domains were purified over a heparin column, eluted in 1 M KCl, subsequently purified on a Rainin HPLC system using a reverse phase C18 column, and chromatographed from 0 to 100% acetonitrile in 0.1% trifluoroacetic acid. The A-RR_{34}-(X) proteins that have the DNA binding region replaced with an acidic extension were purified over a hydroxylapatite column, eluted with a buffer containing 200 mM phosphate, and subsequently purified like the B-ZIP protein domains.

The A-RR_{34}(X) series of proteins expressed differently. The A-RR_{34}(L), A-RR_{34}(N), A-RR_{34}(K), and A-RR_{34}(I) mutants expressed well (6 mg/mL), while the A-RR_{34}(A) and A-RR_{34}(V) proteins expressed poorly in *E. coli*. The solubility of these purified proteins in the CD buffer [12.5 mM potassium phosphate (pH 7.4), 150 mM KCl, and 0.25 mM EDTA] was low. Again the proteins differed in their solubility with A-RR_{34}(N) being the most soluble (the concentration of the saturated protein solution was 37 μM) followed by A-RR_{34}(I), A-RR_{34}(L), A-RR_{34}(K), A-RR_{34}(V), and A-RR_{34}(A) (the concentration of the saturated protein solution was in the range of 3.3−4 μM). Due to the low solubility of the proteins, for our studies we were forced to use the proteins at a very low concentration (2 μM).

Circular Dichroism. Circular dichroism (CD) studies were performed using a Jasco J-720 spectropolarimeter with a 5 mm rectangular CD cell. All protein samples were in 12.5 mM potassium phosphate (pH 7.4), 150 mM KCl, and 0.25 mM EDTA. For the assay, 1 mM DTT was added to the protein solution and heated to 65 °C for 15 min to disrupt any potential disulfide bond between the two cysteine residues in the fifth **d** position, cooled to room temperature for 5 min, and diluted to 2 μM in 1.5 mL of stock buffer (described above). Wavelength scans were performed at 6 °C from 200 to 260 nm. For temperature denaturation studies, the molar ellipticity was recorded at 222 nm continuously from 6 to 80 °C at a scan rate of 1 °C/min.

Thermodynamic Calculations. Values for the melting temperature (T_m) and the enthalpy change at the melting temperature (ΔH_m) were determined from denaturation curves assuming a two-state equilibrium dissociation of α-helical dimers into unfolded monomers. A plot of T_m versus ΔH_m was used to calculate the constant-pressure heat capacity change (ΔC_p) upon denaturation of the zipper. A ΔC_p value of -2.04 ± 0.19 kcal mol^{-1} °C^{-1} was used to calculate ΔG values at 37 °C. The standard errors for T_m and ΔH_m determined from the fitting procedure were typically not higher than ±0.3 °C and ±1.5 kcal/mol, respectively. These errors were individually translated into the error in ΔG_{37} by substituting the extreme T_m and ΔH_m values in the equation for ΔG. We found that the ΔG_{37} values were insensitive to changes in the value of ΔC_p in the error range. The errors for the coupling energies were calculated by taking the sum of the errors in the free energy for the proteins comprising the double-mutant cycle.

Analytical Ultracentrifugation. A Beckman Optima model XL-A analytical ultracentrifuge equipped with a four-place An-Ti rotor was used for sedimentation equilibrium experiments. Three 12 mm cells equipped with carbon-filled, six-channel centerpieces and plane quartz windows were used. The protein samples were mixed in an equimolar concentration, dialyzed, and concentrated to yield three samples with concentrations of 10, 20, and 40 μM (with absorbance at 280 nm being 0.1, 0.2, and 0.4, respectively). Samples were loaded on the right (100 μL/channel) with the corresponding reference buffer on the left (120 μL/channel). The reference buffer contained 12.5 mM potassium phosphate (pH 7.4), 150 mM KCl, 0.25 mM EDTA, and 1 mM β-ME. After equilibration at 3000 rpm and 10 °C at which reference wavelength and radial scans were performed, the rotor was accelerated to the selected experimental speed (24 000 rpm). The scans of protein concentration profiles were collected at 4 h intervals for 40 h. Radial scans were recorded at 280 nm in a step mode with 0.001 cm steps and five averages.

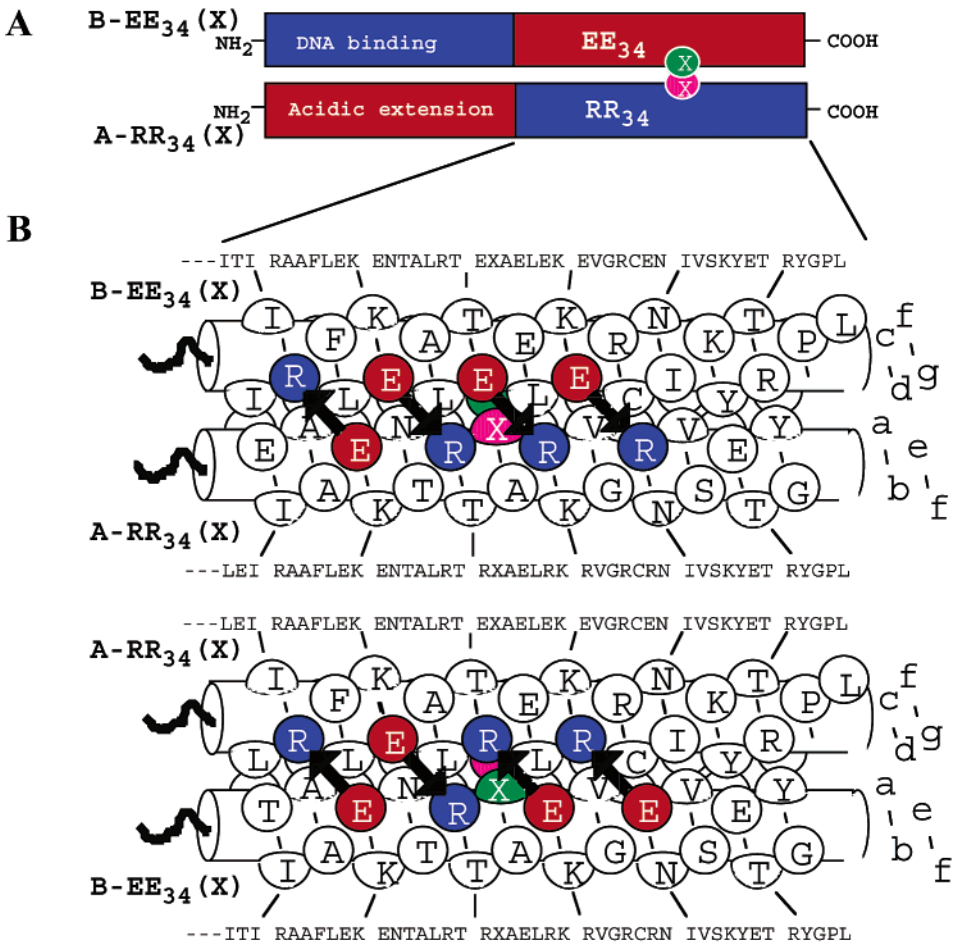

FIGURE 1: (A) Schematic diagram of the guest−host heterodimer. The basic DNA binding region and acidic leucine zipper of B-EE_{34}(X) and the acidic extension and basic leucine zipper of A-RR_{34}(X) are shown with the guest−host third heptad **a** position in the circle. (B) Coiled coil schematic of the heterodimerizing leucine zipper with the amino acids presented in the circles. To the right, the **a**−**g** positions of the leucine zipper coiled coil are identified. The four potential electrostatic interactions between the **g** position of one helix and the following **e′** position of the opposite helix (**g** ↔ **e′** or $i-i'+5$ interaction) are represented by the solid black arrows connecting them. Both sides of the heterodimerizing leucine zipper coiled coil are shown.

Equilibrium was attained typically after 16−20 h, when two consecutive scans taken 4 h apart became indistinguishable. After the data collection had been completed, the rotor was accelerated to 48 000 rpm for 4−5 h and the protein sedimented to the bottom of the cell. The experimental centrifuge speed was restored, and the baseline absorption values were immediately obtained from a single scan. Analysis of ultracentrifugation data was performed with the software package from Beckman, Inc. Partial specific volumes of 0.71 mL/g for all proteins were calculated from amino acid sequences and the values of Zamyatnin (*27*).

RESULTS

Design of Heterodimerizing Leucine Zippers. We have used a heterodimerizing leucine zipper as a guest−host system to generate both homotypic and heterotypic **a**−**a′** interactions. This system allows us to determine the energetic contribution of this position to leucine zipper thermal stability. Figure 1 presents a cartoon of the heterodimerizing guest−host system used in this study that is derived from VBP (*28*), the chicken homologue of mammalian TEF, a member of the PAR family of B-ZIP proteins. The leucine zipper of VBP has four consecutive attractive interhelical **g** ↔ **e′** pairs containing oppositely charged amino acids that stabilize the homodimer. The pattern from the first to the fourth heptad of **g** ↔ **e′** pairs is R ↔ E, E ↔ R, E ↔ R, and E ↔ R. Previously, we generated a heterodimerizing leucine zipper system by changing two of these attractive E ↔ R pairs to repulsive acidic or basic **g** ↔ **e′** pairs (*22*). In one monomer, we changed the third and fourth heptad attractive E ↔ R interhelical pairs to repulsive E ↔ E interhelical pairs to create a molecule termed EE_{34} (R ↔ E, E ↔ R, E ↔ E, and E ↔ E). For the purposes of this paper, we refer to EE_{34} as B-EE_{34}(V). The B represents the basic region of VBP, EE_{34} the VBP leucine zipper with the third and fourth **g** ↔ **e′** pairs containing repulsive E ↔ E interactions, and (V) the valine in the third **a** position. In the second monomer of the heterodimer, we changed the third and fourth heptad attractive **g** ↔ **e′** pairs from E ↔ R to repulsive R ↔ R pairs to create a molecule termed RR_{34} (R ↔ E, E ↔ R, R ↔ R, and R ↔ R) (*22*). However, we were unable to express sufficient quantities of the RR_{34}(X) proteins containing novel amino acids in the third heptad **a** position. To overcome this technical limitation, we replaced the basic region of RR_{34} with an acidic extension to create A-RR_{34}(V) which is expressed well in *E. coli*. The acidic region of A-RR_{34}(V) forms a coiled coil structure with the basic region of B-EE_{34}-(V) stabilizing the heterodimer by 3.9 kcal/mol per dimer

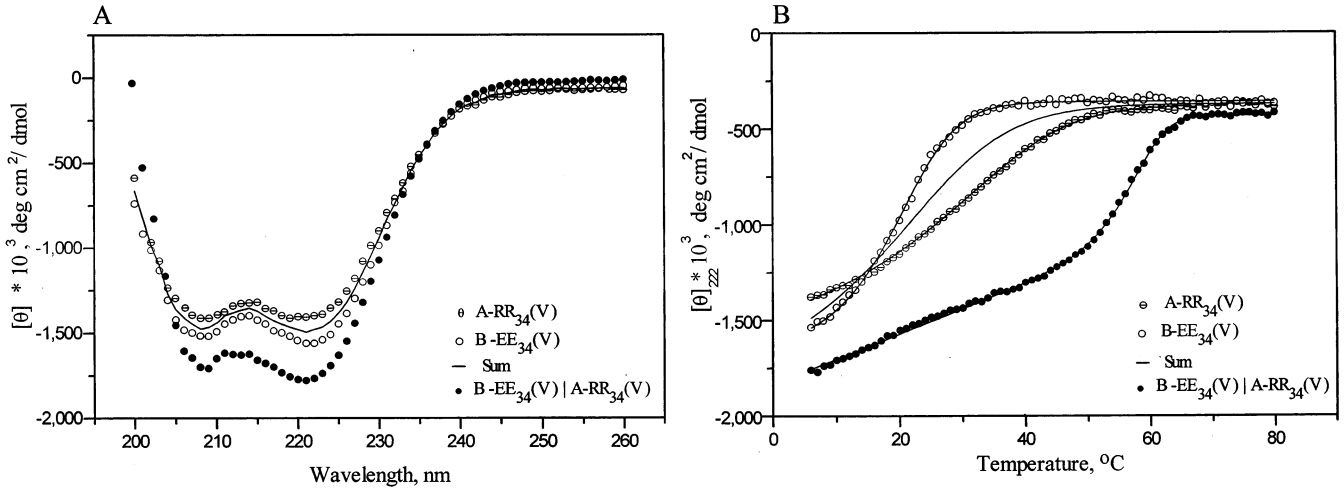

FIGURE 2: (A) Circular dichroism spectra from 200 to 260 nm of B-EE$_{34}$(V) (2 μM), A-RR$_{34}$(V) (2 μM), and the equimolar mixture of 2 μM B-EE$_{34}$(V) and 2 μM A-RR$_{34}$(V). The sum line is the spectrum, assuming the two proteins do not interact. (B) Thermal denaturations monitored by circular dichroism spectroscopy at 222 nm of the samples described for panel A. The B-EE$_{34}$(V)/A-RR$_{34}$(V) mixture is more stable than either protein alone. The line through the data is a fitted curve assuming a two-state equilibrium. The sum line is the expected denaturation curve for the mixture assuming B-EE$_{34}$(V) and A-RR$_{34}$(V) do not interact.

(*24*, *29*). This additional stability makes the difference in homodimer and heterodimer stabilities even greater, thus producing a more versatile guest−host system.

Figure 2A presents circular dichroism (CD) spectra from 200 to 260 nm of B-EE$_{34}$(V) (2 μM), A-RR$_{34}$(V) (2 μM), and the equimolar mixture of B-EE$_{34}$(V) (2 μM) and A-RR$_{34}$-(V) (2 μM). All three spectra exhibit minima at 208 and 222 nm, characteristic of α-helices (*30*). The ratio of ellipticities (222 to 208 nm) is greater than 1.0 and is indicative of interactions between α-helices like those in a coiled coil structure (*31*, *32*). The ellipticity of the mixture is greater than the sum of the ellipticities of the individual samples which we interpret to represent the formation of an α-helical coiled coil structure between the basic region of B-EE$_{34}$(V) and the acidic region of A-RR$_{34}$(V), as has been observed previously (*24*).

Figure 2B presents thermal denaturations monitored by circular dichroism spectroscopy at 222 nm, of the same samples presented in Figure 2A, B-EE$_{34}$(V) (2 μM), A-RR$_{34}$-(V) (2 μM), and the equimolar mixture. B-EE$_{34}$(V) and A-RR$_{34}$(V) have T_ms of 20.5 and 26.5 °C, respectively, while the mixture has a T_m of 57.6 °C. The approximate 30 °C increase in the T_m of the mixture suggests that a heteromeric structure has formed. This reversible denaturation curve fits well assuming a two-state denaturation profile. We calculate that the heterodimer is 7.4 kcal/mol more stable than A-RR$_{34}$-(V) and 9.5 kcal/mol more stable than B-EE$_{34}$(V).

We used analytical ultracentrifugation to determine the oligomerization state of the B-EE$_{34}$(V)−A-RR$_{34}$(V) multimer. These data are best fit to a dimer model with an apparent molecular mass of 21 300 Da (Figure 3 and Table 1) compared to the expected molecular mass of 21 297 Da for the heterodimer.

The preferential thermal stability of the B-EE$_{34}$(V) and A-RR$_{34}$(V) mixture as determined by CD spectroscopy and the dimeric state of the mixture as determined by analytical ultracentrifugation suggest the equimolar mixture is a heterodimer. The 30 °C increase in the stability of the heterodimer relative to the homodimers suggests this is a valuable guest−host system for examining the energetics of

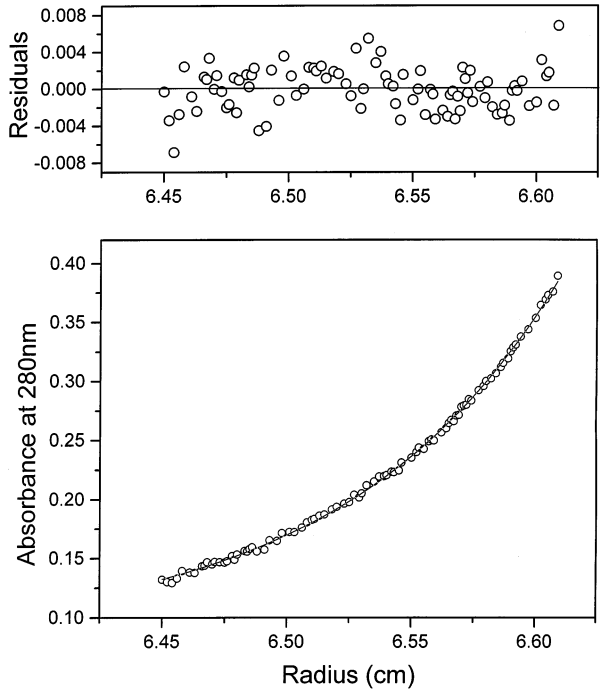

FIGURE 3: Analytical ultracentrifugation of a mixture of B-EE$_{34}$-(V) and A-RR$_{34}$(V) at 6 °C. The theoretical curve for the dimer is plotted as a solid line. The top panel shows the residuals for fitting the experimental data to a dimer model. No systematic error is observed.

both homotypic and heterotypic interactions in the leucine zipper. The large number of structural determinants driving heterodimer formation, (1) the basic region−acidic extension interaction, (2) the attractive **g** ↔ **e′** pairs in the third and fourth heptad that form in the heterodimer, and (3) the presence of an asparagine in the second heptad **a** position, suggest this system will remain dimeric as we change amino acids in the third heptad **a** position.

Mutants. We have chosen the third heptad **a** position as our guest−host position to examine the contribution of different amino acids to dimerization stability and specificity. The third heptad **a** position is flanked by leucines in the second and third heptad **d** positions and attractive interhelical

Table 1: Molecular Masses of Protein Mixtures As Determined by Analytical Ultracentrifugation

protein mixture	MW of the complex[a] (Da)	MW of the heterodimer[b] (Da)
B-EE_{34}(V)/A-RR_{34}(V)	21 300	21 297
B-EE_{34}(V)/A-RR_{34}(N)	22 300	21 312
B-EE_{34}(N)/A-RR_{34}(N)	21 800	21 327
B-EE_{34}(L)/A-RR_{34}(I)	21 800	21 325
B-EE_{34}(L)/A-RR_{34}(N)	23 300	21 326
B-EE_{34}(I)/A-RR_{34}(N)	21 300	21 326

[a] Apparent molecular mass of the protein complex as determined by analytical ultracentrifugation. [b] The expected molecular mass of the equimolar mixture of B-EE_{34}(X) and A-RR_{34}(X).

Table 2: Melting Temperatures (T_m) of the Six B-EE_{34}(X) (2 μM) and Six A-RR_{34}(X) (2 μM) Proteins Determined by Thermal Denaturation Using CD Spectroscopy

	T_m (°C)		
	B-EE_{34}(X)	A-RR_{34}(X)	B-EE_{34}(X) and A-RR_{34}(X)
A	13.8	17.1	40
I	28.1	23.6	61.2
V	20.5	26.5	57.6
L	20.2	22.4	56
N	11.3	14.4	50.1
K	11.0	13.3	25.4

g ↔ **e**′ pairs. This is a typical structural environment found in stable leucine zippers. In both B-EE_{34}(V) and A-RR_{34}(V), we have mutated the V in the third heptad **a** position to A, I, L, N, and K, amino acids that are commonly observed in the **a** position of human B-ZIP proteins (*12*). This heterodimerizing system allows us to produce six homotypic **a**−**a**′ interactions and 30 heterotypic **a**−**a**′ interactions. The 30 heterotypic **a**−**a**′ interactions represent 15 interactions that are each represented twice, e.g., A−I and I−A interactions.

Thermal Stabilities of the 12 Homodimers. The T_ms of the six B-EE_{34}(X) and six A-RR_{34}(X) proteins are presented in Table 2. The most stable protein is B-EE_{34}(I) with a T_m of 28.1 °C. Several of the proteins were so unstable that a low-temperature baseline was undefined which precluded determination of the thermodynamic parameters for these denaturations. The aliphatic amino acids isoleucine, leucine, and valine contribute more to stability than alanine, asparagine, and lysine. The general pattern of stabilities is similar to what we expect from previous studies in which homotypic interactions in the **a** position of coiled coils were examined (*19*).

*Thirty-Six **a**−**a**′ Interactions Produced by Heterodimers.* We have mixed the six B-EE_{34}(X) proteins with the six A-RR_{34}(X) proteins to create 36 heterodimers. The ratio of ellipticities (222 to 208 nm) was greater than 1.0 in all cases, suggesting the heterodimers are forming a coiled coil structure. Also, the mixture was dramatically more stable than either of the homodimers, suggesting the mixtures are heteromers. To ascertain the oligomeric state, we performed analytical ultracentrifugations with five mixtures that produced the **a**−**a**′ interactions (V−N, N−N, L−I, L−N, and I−N). In all cases, the mixtures are dimeric (Table 1).

Thermal denaturations of these 36 mixtures, monitored by circular dichroism spectroscopy at 222 nm, are fit well by a two-state denaturation model, allowing thermodynamic parameters to be determined (Table 3). Figure 4 presents

Table 3: Thermal Stabilities [ΔG_{37} (kcal/mol)] of Heterodimerizing Proteins[a]

	A-RR_{34}(A)			A-RR_{34}(I)			A-RR_{34}(V)			A-RR_{34}(L)			A-RR_{34}(N)			A-RR_{34}(K)		
	T_m (°C)	ΔH_m (kcal/mol)	ΔG_{37} (kcal/mol)	T_m (°C)	ΔH_m (kcal/mol)	ΔG_{37} (kcal/mol)	T_m (°C)	ΔH_m (kcal/mol)	ΔG_{37} (kcal/mol)	T_m (°C)	ΔH_m (kcal/mol)	ΔG_{37} (kcal/mol)	T_m (°C)	ΔH_m (kcal/mol)	ΔG_{37} (kcal/mol)	T_m (°C)	ΔH_m (kcal/mol)	ΔG_{37} (kcal/mol)
B-EE_{34}(A)	40.0	−57.3	−9.3 ± 0.1	55.0	−102	−13.3 ± 0.06	49.7	−100.5	−11.7 ± 0.06	51.1	−83.3	−11.6 ± 0.1	46.0	−83.4	−10.3 ± 0.1	26.0	−30.5	−7.7 ± 0.13
B-EE_{34}(I)	55.4	−106.5	−13.6 ± 0.06	61.2	−126	−18.5 ± 0.07	58.2	−111.7	−15.6 ± 0.07	60.5	−100.7	−15.0 ± 0.03	45.2	−71.1	−9.7 ± 0.04	48.9	−93.3	−12.4 ± 0.05
B-EE_{34}(V)	49.2	−104.1	−11.6 ± 0.07	58.0	−119	−15.4 ± 0.1	57.6	−111.2	−14.7 ± 0.02	55.7	−102	−13.7 ± 0.03	43.4	−81	−9.4 ± 0.01	51.0	−93.4	−10.5 ± 0.02
B-EE_{34}(L)	49.7	−89.1	−11.6 ± 0.04	60.6	−100	−15.1 ± 0.1	56.0	−105	−13.8 ± 0.1	58.5	−104.6	−14.5 ± 0.04	45.0	−76.1	−9.8 ± 0.05	43.7	−78.8	−10.1 ± 0.03
B-EE_{34}(N)	46.6	−78.2	−10.2 ± 0.05	47.3	−51.2	−9.9 ± 0.08	43.8	−89.8	−9.6 ± 0.02	45.0	−79.5	−9.9 ± 0.03	50.1	−99.3	−11.7 ± 0.01	37.6	−67.2	−8.8 ± 0.03
B-EE_{34}(K)	34.2	−74.1	−8.3 ± 0.1	51.2	−90.2	−13 ± 0.06	46.3	−91.1	−11.2 ± 0.1	46.0	−77	−10.8 ± 0.03	43.7	−88.1	−9.6 ± 0.03	25.4	−48.5	−6.4 ± 0.2

[a] Thermodynamic characterizations of the thermal denaturation profiles assuming a two-state denaturation: the thermal stability measured by circular dichroism at 222 nm, including the melting temperature (T_m, °C), the enthalpy change at the melting temperature (ΔH_m, kcal/mol), and the dimerization free energy extrapolated to 37 °C (ΔG_{37}, kcal/mol). The standard errors for T_m and ΔH_m determined from the fitting procedure were typically not higher than 0.3 °C and 1.5 kcal/mol, respectively. These errors were individually translated into the error in ΔG_{37} by substituting the extreme T_m and ΔH_m values in the equation for ΔG_{37}.

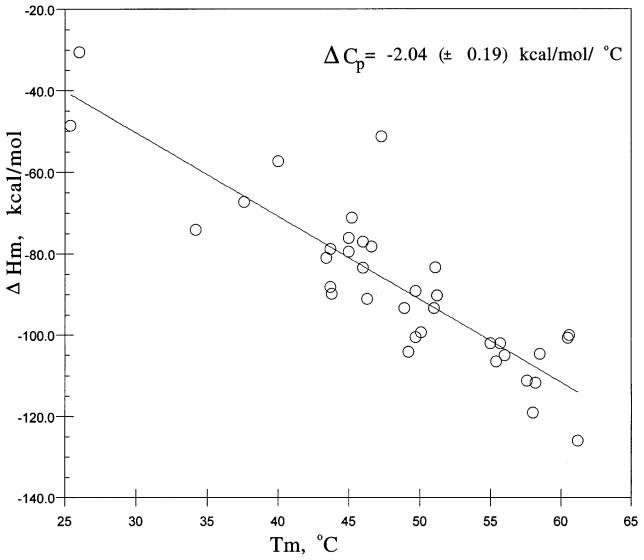

FIGURE 4: Plot of ΔH_m (the enthalpy change at the melting temperature) vs T_m (the melting temperature) for calculating the ΔC_p (the constant-pressure heat capacity change) for the 36 protein mixtures thermally denatured.

the T_m versus ΔH_m plot for all 36 denaturations presented in this paper. A line fitted through these data has a slope (ΔC_p) of -2.04 ± 0.19 kcal mol^{-1} °C^{-1}. This is greater than the ΔC_p (-1.2 kcal mol^{-1} °C^{-1}) we have observed for a series of mutations in the **g** and **e** positions of VBP (*22*). The heterodimer coiled coil structure between the basic region of B-EE$_{34}$(X) and the acidic region of A-RR$_{34}$(X) generates additional hydrophobic surface in the heterodimer which would be expected to increase the ΔC_p value. Using this calculated ΔC_p, we have calculated a ΔG_{37} value for each of the 36 denaturations (Table 3). From the ΔG_{37} values presented in Table 3, the stabilities of the 35 **a**−**a′** interactions relative to the A−A interaction ($\Delta\Delta G$) were calculated (Table 4).

There are six heterodimer mixtures that produce homotypic **a**−**a′** interactions. The thermal stabilities ranged from a T_m of 25.4 °C for the B-EE$_{34}$(K)/A-RR$_{34}$(K) mixture that produced a K−K interaction to 61.2 °C for the B-EE$_{34}$(I)/A-RR$_{34}$(I) mixture that produced an I−I interaction. The fraction of monomer for these six denaturations is presented in Figure 5. The stabilities of these **a**−**a′** interactions relative to the A−A interaction are listed in Table 4. The descending order of stability is as follows: isoleucine is 9.2 kcal/mol per dimer, valine 5.4 kcal/mol per dimer, leucine 5.2 kcal/mol per dimer, and asparagine 2.4 kcal/mol per dimer more stable than the A−A interaction. The K−K interaction is 2.9 kcal/mol per dimer less stabilizing than the A−A interaction.

The mixture of six B-EE$_{34}$(X) proteins and six A-RR$_{34}$-(X) proteins creates 30 heterotypic **a**−**a′** interactions. As with the homotypic interactions, CD spectra for each heterodimer show a 222 to 208 nm ratio of >1.0, suggestive of a coiled coil structure. Figure 6 shows that the V−N heterotypic interaction is less stable than either the N−N or V−V homotypic interactions, but none of the heterotypic interactions are as unstable as the K−K interaction or as stable as the I−I interaction.

The 30 heterotypic interactions contain two versions of each of 15 different **a**−**a′** interactions. Because we have placed each of the six amino acids in both the B-EE$_{34}$(X) and A-RR$_{34}$(X) background, the mixture of these proteins produces reciprocal heterotypic **a**−**a′** interactions. For example, we produce both an A−I and an I−A interaction. These two reciprocal heterotypic interactions are not structurally equivalent, but they are similar, as seen schematically in Figure 7. The flanking **d** positions are identical, but the surrounding **g** ↔ **e′** pairs are different. The majority of the reciprocal interactions are energetically similar; e.g., the V−I and I−V interactions differ by only 0.2 kcal/mol per dimer, suggesting that the energetics of these interactions are not dependent on surrounding structural elements. The similarity of the energetics of the reciprocal heterotypic interactions also provides great confidence that the measurements are accurate.

The **a**−**a′** pairs containing alanine allow an examination of the contribution of a single amino acid in the **a**−**a′** pairs to stability. All the amino acids are stabilizing relative to alanine except K. Among the aliphatic amino acids, isoleucine is 2.0 kcal/mol more stabilizing than either valine or leucine. The extra methylene in isoleucine relative to valine may be interacting intrahelically with the leucines in the neighboring **d** positions.

Reciprocal **a**−**a′** interactions containing K show the greatest difference. In all five heterotypic **a**−**a′** pairs containing K, when K is in B-EE$_{34}$(K), the **a**−**a′** pairs are 0.6−0.8 kcal/mol per dimer more stable than the reciprocal **a**−**a′** pair with K in A-RR$_{34}$(K). The B-EE$_{34}$(K) conformation is what is observed in the FOS leucine zipper, where the lysine in the **a** position is surrounded by glutamic acids in the **g** and **e** positions. X-ray crystal structures of the FOS−JUN heterodimer indicate that a buried lysine makes intrahelical contacts with the negatively charged **e** or **g** position (*33*, *34*).

*Calculated Coupling Energies for **a**−**a′** Interactions.* We have used an alanine-based double-mutant thermodynamic cycle to calculate coupling energies for the **a**−**a′** interaction (*35*) (Table 5). All the homotypic interactions except those of K have a negative coupling energy, suggesting the amino acids interact with each other to stabilize the structure. The magnitude of the coupling energy however is small, less than -1.0 kcal/mol per dimer. This is similar to the measured coupling energies for attractive interhelical **g** ↔ **e′** pairs between E and R (*23*). The K−K coupling energy is slightly destabilizing at 0.3 kcal/mol per dimer, indicating that the lysines in the **a**−**a′** pair do not interact to destabilize the structure. In contrast, lysines in the **g** ↔ **e′** pairs are more repulsive with a coupling energy of 0.6 kcal/mol per dimer (*23*).

The heterotypic **a**−**a′** coupling energies are all destabilizing except for those containing K. The heterotypic aliphatic (V−I, V−L, and I−L) coupling energies are slightly destabilizing which is in contrast to the homotypic interactions which are slightly stabilizing. The most destabilizing **a**−**a′** coupling energies contain asparagine and an aliphatic amino acid, ranging from 4.9 kcal/mol per dimer for an I−N interaction to 2.8 kcal/mol per dimer for an L−N interaction. This is in contrast to the small stabilizing coupling energy of -0.5 kcal/mol per dimer for the N−N interaction. Lysine, in contrast, has only small stabilizing coupling energies in all its heterotypic **a**−**a′** interactions which are all in the range of -0.2 to -0.7 kcal/mol per dimer.

Table 4: Energetic Stability ($\Delta\Delta G$) of Homotypic and Heterotypic **a**−**a′** Interactions Relative to That of an A−A Interaction[a]

	$\Delta\Delta G_{37}$ (kcal/mol)					
	A-RR_{34}(A)	A-RR_{34}(I)	A-RR_{34}(V)	A-RR_{34}(L)	A-RR_{34}(N)	A-RR_{34}(K)
B-EE_{34}(A)	0.0	−4.0 ± 0.16	−2.4 ± 0.16	−2.3 ± 0.2	−1.0 ± 0.2	**1.6 ± 0.23**
B-EE_{34}(I)	−4.3 ± 0.16	−9.2 ± 0.17	−6.3 ± 0.17	−5.7 ± 0.13	−0.4 ± 0.14	−3.1 ± 0.15
B-EE_{34}(V)	−2.3 ± 0.17	−6.1 ± 0.2	−5.4 ± 0.12	−4.4 ± 0.13	−0.1 ± 0.11	−1.2 ± 0.12
B-EE_{34}(L)	−2.3 ± 0.14	−5.8 ± 0.2	−4.5 ± 0.2	−5.2 ± 0.14	−0.5 ± 0.15	−0.8 ± 0.13
B-EE_{34}(N)	−0.9 ± 0.15	−0.6 ± 0.18	−0.3 ± 0.12	−0.6 ± 0.13	−2.4 ± 0.11	**0.5 ± 0.13**
B-EE_{34}(K)	**1.0 ± 0.2**	−3.7 ± 0.16	−1.9 ± 0.2	−1.5 ± 0.13	−0.3 ± 0.13	**2.9 ± 0.3**

[a] The thermal stabilities of the 35 heterodimers were calculated relative to the thermal stability of alanine [B-EE_{34}(A)/A-RR_{34}(A)] from the ΔG_{37} values presented in Table 3. Interactions that are less stable than the alanine **a**−**a′** interaction are depicted in bold.

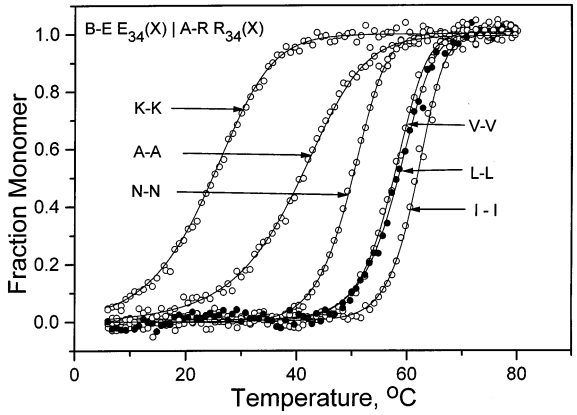

FIGURE 5: Monomer fractions of the six heterodimer denaturations that create homotypic **a**−**a′** interactions.

DISCUSSION

We have examined the energetic contribution to dimerization stability and specificity of six amino acids (I, V, L, N, A, and K) in the **a** position of the leucine zipper. Amino acids in the **a** position can interact interhelically to produce an **a**−**a′** interaction. To measure the coupling energy of this interaction, we have used a heterodimerizing system based on the VBP leucine zipper. The heterodimerizing system allows us to study both homotypic and heterotypic **a**−**a′** interactions. Thus, we can complete an alanine-based double-mutant thermodynamic cycle and calculate the coupling energy between amino acids in the **a** and **a′** positions. We have measured the thermal stability of 36 heterodimers which contain six homotypic and 30 heterotypic **a**−**a′** interactions. These data help unravel the structural rules that determine the contribution of **a** position amino acids to the dimerization specificity of leucine zipper coiled coils.

Experiments that vary amino acids in the **a** position are complicated because they can modulate oligomerization (*15*, *16*). To avoid this complication, we used a system in which the other structural elements favor dimerization. To preserve the dimeric structure, we avoided changing the asparagine in the second heptad **a** position of the guest host system; instead, we mutated the valine in the third heptad **a** position. To add additional dimerization determinants to the heterodimerizing system, we replaced the basic region of RR_{34}-(X) with an acidic region to generate A-RR_{34}(X). This acidic extension forms a coiled coil heterodimer with the basic region of B-EE_{34}(X). In all the mutants we examined, this system creates heterodimers.

Among the homotypic **a**−**a′** interactions, the hydrophobic amino acid I−I, V−V, and L−L interactions are 9.2, 5.4, and 5.2 kcal/mol per dimer, respectively, more stable than an A−A interaction. If an amino acid's energetic contribution to stability is greater than the transfer free energy, which is

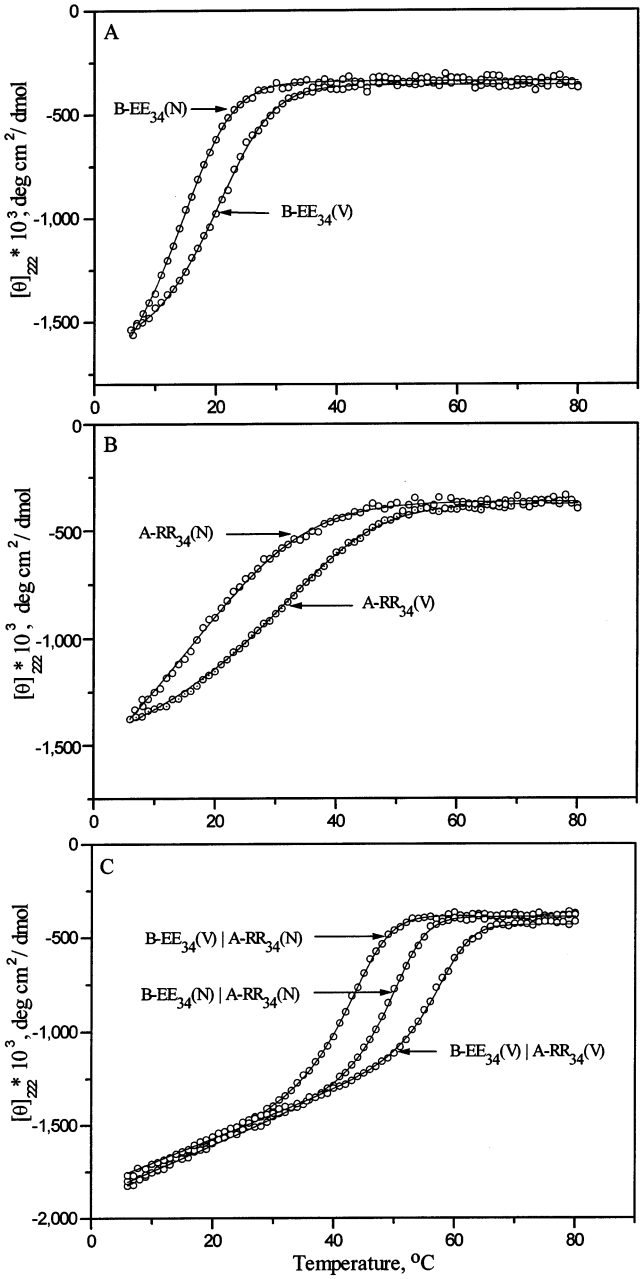

FIGURE 6: Circular dichroism thermal denaturations of proteins monitored at 222 nm: (A) 2 μM B-EE_{34}(V) and 2 μM B-EE_{34}(N), (B) 2 μM A-RR_{34}(V) and 2 μM A-RR_{34}(N), and (C) B-EE_{34}(V)−A-RR_{34}(V), B-EE_{34}(N)−A-RR_{34}(N), and B-EE_{34}(V)−A-RR_{34}(N) heterodimers where each monomeric protein was at a concentration 2 μM.

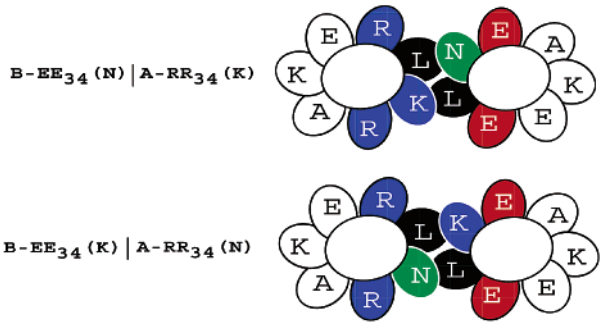

FIGURE 7: Cartoon of an end view of heterodimers that produce reciprocal **a**−**a′** interactions that are energetically the most different [B-EE$_{34}$(N)−A-RR$_{34}$(K) and B-EE$_{34}$(K)−A-RR$_{34}$(N)].

Table 5: Coupling Energies ($\Delta\Delta\Delta G$) for the **a**−**a′** Interactions Relative to That of an A−A Interaction[a]

	$\Delta\Delta\Delta G_{37}$ (kcal/mol)				
	A-RR$_{34}$(I)	A-RR$_{34}$(V)	A-RR$_{34}$(L)	A-RR$_{34}$(N)	A-RR$_{34}$(K)
B-EE$_{34}$(I)	−0.9	**0.4**	**0.9**	**4.9**	−0.4
B-EE$_{34}$(V)	**0.2**	−0.7	**0.2**	**3.2**	−0.5
B-EE$_{34}$(L)	**0.5**	**0.2**	−0.6	**2.8**	−0.1
B-EE$_{34}$(N)	**4.3**	**3.0**	**2.6**	−0.5	−0.2
B-EE$_{34}$(K)	−0.7	−0.5	−0.2	−0.3	**0.3**

[a] The coupling energies of the 25 heterodimers relative to alanine were calculated using the $\Delta\Delta G$ values presented in Table 4. The error for the coupling energies is given by the sum of the errors in the free energy for the proteins comprising the double-mutant cycle and was calculated to be approximately ±0.5 kcal/mol. Positive coupling energy has been highlighted in bold.

Table 6: Estimation of the van der Waals Contacts for Amino Acids in the **a**−**a′** Interaction[a]

amino acid	$\Delta\Delta G_A$ (kcal/mol)	$\Delta\Delta G_{helix}$ (kcal/mol)	$\Delta\Delta G_A - \Delta\Delta G_{helix}$ (kcal/mol)	$\Delta\Delta G_{transfer}$ (kcal/mol)	$\Delta\Delta G_{packing}$ (kcal/mol)
L−L	−2.25	0.15	−2.40	−2.32	−0.08
I−I	−4.6	0.54	−5.14	−2.46	−2.68
V−V	−2.7	0.63	−3.33	−1.66	−1.67
A−A	0.0	0.0	0.0	−0.42	0.0
K−K	1.45	0.08	1.37	1.35	0.02
N−N	−1.2	0.7	−1.9	0.82	−2.72

[a] $\Delta\Delta G_A$ is the free energy of unfolding for a single amino acid in the monomer relative to alanine. $\Delta\Delta G_{helix}$ is the helical propensity of amino acids relative to alanine (*48*). $\Delta\Delta G_{transfer}$ values are the transfer free energy values from ref *49*. The difference between $\Delta\Delta G_A$ and the sum of $\Delta\Delta G_{transfer}$ and $\Delta\Delta G_{helix}$ is defined as the free energy of packing ($\Delta\Delta G_{packing}$).

a measure of the entropic effect or hydrophobicity, it suggests the amino acid is uniquely packing in the structure (Table 6). This analysis suggests that the contribution of V and L to stability is similar to their transfer free energy. In contrast, the contribution of I to stability is more than twice the transfer free energy, suggesting that I has some unique packing properties. Isoleucine in the I−A and the A−I **a**−**a′** pairs also shows a stability greater than the transfer free energy, indicating that the packing of I is not from the I−I **a**−**a′** pair. Possible packing occurs with the intrahelical leucines in the **d** and **d′** positions.

A dramatic difference in the contribution of aliphatic amino acids to stability is also observed in the **d** position of a coiled coil (*36*). In this position, it is leucine, not isoleucine, that contributes more to stability than the transfer free energy would predict.

Hodges and co-workers have also examined the energetic contribution of homotypic **d**−**d′** and **a**−**a′** interactions (*19*, *37*) to dimeric coiled coil stability. Their experiments show a preference for leucine in the **d** position, being 0.4 kcal/mol per residue more stable than isoleucine which is not as dramatic a difference as we observe with leucine being 2.95 kcal/mol per residue more stable than isoleucine (*36*). The Hodges model coiled coil system indicates that valine is the most stable aliphatic amino acid in the **a** position, being 0.2 kcal/mol per residue more stable than isoleucine. This result is in clear contrast to the data reported here where isoleucine is 1.9 kcal/mol per residue more stable than valine. Table 7 presents a comparison of these data. The Hodges model system has a glycine in the **b** position of each heptad that may weaken the rigid α-helix of the coiled coil. This could allow more conformational flexibility and hydrophobic repacking of the **a** and **d** positions and thus blurring of the differences between amino acids. The natural VBP leucine zipper in contrast does not contain glycines which should result in more rigid α-helices that could reveal the different properties of amino acids in the core of the coiled coil. However, when we (*22*, *23*) and Hodges and co-workers (*38*) use our different model systems to examine the contribution of the **g** and **e** positions to protein stability, we come to similar conclusions. This suggests that the energetics of interhelical electrostatic interactions are not sensitive to potential packing rearrangements.

Our study of the **a** position contributes to the systematic studies of leucine zipper coiled coils that have examined which amino acids are most stabilizing in the **a**, **d**, **e**, and **g**, positions, the four positions that can interact interhelically. On the basis of these data, the most stabilizing leucine zipper would have isoleucine in the **a** position, leucine in the **d** position (*36*), glutamic acid in the **g** position, and arginine in the **e** position (*23*). A two-heptad leucine zipper has been designed that uses this collection of four amino acids (*39*, *40*) and may represent the most stable coiled coil.

Coupling energy calculations reveal how the **a**−**a′** interaction of the coiled coil contributes to dimerization specificity. The three aliphatic homotypic **a**−**a′** interactions (V−V, L−L, and I−I) stabilize the structure with a negative coupling energy ranging from −0.6 to −0.9 kcal/mol per dimer. These are of the same magnitude as the measured coupling energy for the interhelical attractive **g** ↔ **e′** interaction. In contrast, the aliphatic heterotypic **a**−**a′** interactions (V−I, V−L, I−L, I−V, L−V, and L−I) have a positive coupling energy ranging from 0.23 to 0.9 kcal/mol per dimer. Without a high-resolution structure of these interactions, the physical basis of the negative coupling energy for the homotypic interactions is obscure. One possibility is that the homotypic interactions contribute to coiled coil symmetry which is stabilizing, while the heterotypic interactions disrupt the coiled coil symmetry and thus are destabilizing.

The asparagine side chains in the **a**−**a′** interaction are seen in both X-ray (*7*) and NMR (*41*, *42*) structures to form an intersubunit hydrogen bond surrounded by a hydrophobic surface composed of the **d** position amino acids. The coupling energy of this interhelical interaction, however, has not been measured previously in either the homotypic N−N interaction or the heterotypic N−X interactions. Our measurements indicate that the coupling energy of the N−N interaction is −0.5 kcal/mol per dimer. Comparing the

Table 7: Comparison of the **a** and **d** Positions

amino acid	$\Delta\Delta G_A$ at the **a** position[a] (kcal/mol)	$\Delta\Delta G_A$ at the **d** position[b] kcal/mol)	positional difference **a** − **d**[c] (kcal/mol)	$\Delta\Delta G_A$ at the **a** position, Hodges' data[d] (kcal/mol)	$\Delta\Delta G_A$ at the **d** position, Hodges' data[e] (kcal/mol)	positional difference **a** − **d**[f] (kcal/mol)	$\Delta\Delta G_{transfer\ free\ energy}$[g] (kcal/mol)
I	−4.6	−1.65	−2.95	−1.95	−1.5	−0.45	−2.46
V	−2.7	−1.1	−1.6	−2.05	−0.55	−1.5	−1.66
L	−2.6	−4.6	2.0	−1.75	−1.9	0.15	−2.32
N	−1.2	−	−	−0.45	0.3	−0.75	0.82
A	0.0	0.0	0.0	0.0	0.0	0.0	−0.42
K	1.45	−	−	0.2	0.9	−0.7	1.35

[a] Stability contribution per residue relative to alanine in the **a** position (data from this study). [b] Stability of amino acids in the **d** position using the VBP B-ZIP domain as the guest−host system (*36*). [c] Difference in the contribution to stability of amino acids in the **a** and **d** positions. [d] Stability contribution of amino acids in the **a** position using a model coiled coil system (*19*). [e] Stability contribution of amino acids in the **d** position using a model coiled coil system (*37*). [f] Difference in the contribution to stability of amino acids in the **a** and **d** positions (the model system data). [g] Transfer free energy of amino acids for transfer from water to octanol relative to glycine which is a measure of hydrophobicity (*49*).

stability of the N−A, A−N, N−N, I−N, and N−I **a**−**a**′ pairs and the coupling energy of the N−N, I−N, and N−I **a**−**a**′ pairs gives some insight into the physical basis of the coupling energies. The relatively small −0.5 kcal/mol coupling energy of the N−N pair suggests that asparagine in the N−A, A−N, and N−N pairs is in a hydrophilic environment. In the N−A pair, asparagine hydrogen bonds with water, while in the N−N pair, asparagine hydrogen bonds with the second asparagine in the N−N pair. The crystal structure of the APC tumor suppressor shows an A−A **a**−**a**′ pair contains water molecules in the interior of the interface (*43*). In the N−I and I−N pairs, however, asparagine is unable to hydrogen bond because it is buried in a hydrophobic environment, resulting in a coupling energy for the N−I interaction that is destabilizing (4.3 kcal/mol). The one aspect of this description that is unexpected is the low coupling energy of the I−I pair. One might have expected that if the N−I pair buried the N which is energetically costly then the I−I pair would have buried the I, resulting is a more significant calculated coupling energy for the I−I pair.

It was demonstrated earlier, but only in a qualitative way, that buried asparagines in the dimer interface can determine dimerization specificity (*20*). This analysis shows quantitatively that asparagine can regulate dimerization specificity by preventing heterodimerization with aliphatic amino acids. This "negative design" which was first theorized by Hurst (*44*) is also observed in the **g** and **e** positions of the leucine zipper coiled coil (*45*, *46*). The preferential heterodimerization of the FOS and JUN leucine zippers is because of the repulsive interhelical **g** ↔ **e**′ pairs containing glutamate that prevent FOS homodimerization, helping to drive heterodimerization with JUN. We measure a positive coupling energy for the E ↔ E **g** ↔ **e**′ pair of 0.8 kcal/mol, while the E ↔ R **g** ↔ **e**′ pair has a negative coupling energy of −0.5 kcal/mol (*23*). Thus, it appears that coiled coil dimerization specificity in both the **g** ↔ **e**′ interaction and the **a**−**a**′ interaction is primarily governed by preventing repulsive interactions.

A recent examination of the B-ZIP proteins in both the *Drosophila* (*47*) and human (*12*) genomes showed that asparagine is common in the **a** position of B-ZIP proteins. As has been observed previously, asparagine occurs in the second heptad **a** position of most B-ZIP proteins, including all homodimerizing proteins. In both *Drosophila* and humans, asparagine is found in the fourth heptad **a** position and the third and fifth heptad **a** positions of the homodimerizing Oasis and ATF6 families of B-ZIP proteins, respectively. Thus, it appears that asparagine has been used to define new homodimerizing B-ZIP proteins throughout metazoan life by inhibiting interactions with leucine zippers that do not produce N−N homotypic interactions.

We know of two structural situations that are used by B-ZIP leucine zippers that prevent heterodimerization. One is to have proteins with **g** ↔ **e**′ pairs that are opposite in orientation. For example, if one partner has an E ↔ R **g** ↔ **e**′ pair and the second partner has an R ↔ E **g** ↔ **e**′ pair, the heterodimer is disfavored because it produces a repulsive E ↔ E **g** ↔ **e**′ pair and a repulsive R ↔ R **g** ↔ **e**′ pair. We calculate this would destabilize heterodimerization with PAR proteins containing an E ↔ R salt bridge in the third position by 2.9 kcal/mol (*23*). Reversal of a single salt bridge has been shown experimentally to prevent heterodimerization (*24*). The second situation is described in this paper. The placement of N in the **a** position can produce a stabilizing homotypic N−N **a**−**a**′ interaction, but the heterotypic interaction with the aliphatic amino acids, the typical amino acids in this location of a leucine zipper, is disfavored. Interestingly, the energetic cost of forming a heterodimer with the N−V **a**−**a**′ pair is similar to the cost of forming a heterodimer with a repulsive E ↔ E **g** ↔ **e**′ pair and a repulsive R ↔ R **g** ↔ **e**′ pair.

Of the six amino acids examined in the **a** position, only lysine preferred to form heterotypic interactions. Lysine is found in the **a** position of all the heterodimerizing B-ZIP proteins, including FOS, CNC, and L-MAF. Lysine is in the **a** position of the second and fourth heptads of FOS, the second and third heptads of CNC, and the first heptad of L-MAF. The FOS−JUN heterodimer forms a K−N **a**−**a**′ interaction in the second heptad and a K−V **a**−**a**′ interaction in the fourth heptad. Our measurements suggest that lysine does not discriminate between the K−N and K−V heterotypic **a**−**a**′ interaction.

The heterodimerizing guest−host system we introduce in this paper has been used to assess homotypic and heterotypic **a**−**a**′ interactions. These data demonstrate that the **a** position of the leucine zipper can favor either homodimerization or heterodimerization.

ACKNOWLEDGMENT

We thank Dmitry Krylov and Vikas Rishi for advice and encouragement.

REFERENCES

1. Landschultz, W. H., Johnson, P. F., and McKnight, S. L. (1988) *Science 240*, 1759−1764.
2. Vinson, C. R., Sigler, P. B., and McKnight, S. L. (1989) *Science 246*, 911−916.
3. Alber, T. (1992) *Curr. Opin. Genet. Dev. 2*, 205−210.
4. Baxevanis, A., and Vinson, C. (1993) *Curr. Opin. Genet. Dev. 3*, 278−285.
5. Lupas, A. (1996) *Trends Biochem. 21*, 375−382.
6. Burkhard, P., Strelkov, S. V., and Stetefeld, J. (2001) *Trends Cell Biol. 11*, 82−88.
7. O'Shea, E. K., Klemm, J. D., Kim, P. S., and Alber, T. (1991) *Science 254*, 539−544.
8. Ellenberger, T., Brandl, C., Struhl, K., and Harrison, S. (1992) *Cell 71*, 1223−1237.
9. McLachlan, A., and Stewart, M. (1975) *J. Mol. Biol. 98*, 293−304.
10. Crick, F. (1953) *Acta Crystallogr. 6*, 689−697.
11. Thompson, K. S., Vinson, C. R., and Freire, E. (1993) *Biochemistry 32*, 5491−5496.
12. Vinson, C., Myakishev, M., Acharya, A., Mir, A. A., Moll, J. R., and Bonovich, M. (2002) *Mol. Cell. Biol. 22*, 6321−6335.
13. Lupas, A., Van Dyke, M., and Stock, J. (1991) *Science 252*, 1162−1164.
14. Cohen, C., and Parry, D. A. (1990) *Proteins 7*, 1−15.
15. Harbury, P. B., Zhang, T., Kim, P. S., and Alber, T. (1993) *Science 262*, 1401−1407.
16. Potekhin, S. A., Medvedkin, V. N., Kashparov, I. A., and Venyaminov, S. (1994) *Protein Eng. 7*, 1097−1101.
17. Gonzalez, L., Jr., Woolfson, D. N., and Alber, T. (1996) *Nat. Struct. Biol. 3*, 1011−1018.
18. Wagschal, K., Tripet, B., and Hodges, R. S. (1999) *J. Mol. Biol. 285*, 785−803.
19. Wagschal, K., Tripet, B., Lavigne, P., Mant, C., and Hodges, R. S. (1999) *Protein Sci. 8*, 2312−2329.
20. Zeng, X., Herndon, A. M., and Hu, J. C. (1997) *Proc. Natl. Acad. Sci. U.S.A. 94*, 3673−3678.
21. Zhu, H., Celinski, S. A., Scholtz, J. M., and Hu, J. C. (2000) *J. Mol. Biol. 300*, 1377−1387.
22. Krylov, D., Mikhailenko, I., and Vinson, C. (1994) *EMBO J. 13*, 1849−1861.
23. Krylov, D., Barchi, J., and Vinson, C. (1998) *J. Mol. Biol. 279*, 959−972.
24. Moll, J. R., Olive, M., and Vinson, C. (2000) *J. Biol. Chem. 275*, 34826−34832.
25. Studier, F. W., and Moffatt, B. A. (1986) *J. Mol. Biol. 189*, 113−130.
26. Olive, M., Krylov, D., Echlin, D. R., Gardner, K., Taparowsky, E., and Vinson, C. (1997) *J. Biol. Chem. 272*, 18586−18594.
27. Zamyatnin, A. (1984) *Annu. Rev. Biophys. Bioeng. 13*, 145−165.
28. Iyer, S. V., Davis, D. L., Seal, S. N., and Burch, J. B. (1991) *Mol. Cell. Biol. 11*, 4863−4875.
29. Krylov, D., Olive, M., and Vinson, C. (1995) *EMBO J. 14*, 5329−5337.
30. Chen, Y. H., Yang, J. T., and Chau, K. H. (1974) *Biochemistry 13*, 3350−3359.
31. Lau, S. Y., Taneja, A. K., and Hodges, R. S. (1984) *J. Biol. Chem. 259*, 13253−13261.
32. Cooper, T. M., and Woody, R. W. (1990) *Biopolymers 30*, 657−676.
33. Woolfson, D. N., and Alber, T. (1995) *Protein Sci. 4*, 1596−1607.
34. Glover, J. N., and Harrison, S. C. (1995) *Nature 373*, 257−261.
35. Serrano, L., Horovitz, A., Avron, B., Bycroft, M., and Fersht, A. R. (1990) *Biochemistry 29*, 9343−9352.
36. Moitra, J., Szilak, L., Krylov, D., and Vinson, C. (1997) *Biochemistry 36*, 12567−12573.
37. Tripet, B., Wagschal, K., Lavigne, P., Mant, C. T., and Hodges, R. S. (2000) *J. Mol. Biol. 300*, 377−402.
38. Zhou, N. E., Kay, C. M., and Hodges, R. S. (1994) *Protein Eng. 7*, 1365−1372.
39. Burkhard, P., Meier, M., and Lustig, A. (2000) *Protein Sci. 9*, 2294−2301.
40. Burkhard, P., Ivaninskii, S., and Lustig, A. (2002) *J. Mol. Biol. 318*, 901−910.
41. Saudek, V., Pastore, A., Castiglione Morelli, M. A., Frank, R., Gausepohl, H., Gibson, T., Weih, F., and Roesch, P. (1990) *Protein Eng. 4*, 3−10.
42. Saudek, V., Pastore, A., Morelli, M. A., Frank, R., Gausepohl, H., and Gibson, T. (1991) *Protein Eng. 4*, 519−529.
43. Day, C. L., and Alber, T. (2000) *J. Mol. Biol. 301*, 147−156.
44. Hurst, H. C. (1995) *Protein Profile 2*, 101−168.
45. Nicklin, M. J., and Casari, G. (1991) *Oncogene 6*, 173−179.
46. O'Shea, E. K., Rutkowski, R., and Kim, P. S. (1992) *Cell 68*, 699−708.
47. Fassler, J., Landsman, D., Acharya, A., Moll, J. R., Bonovich, M., and Vinson, C. (2002) *Genome Res. 12*, 1190−1200.
48. O'Neil, K. T., and DeGrado, W. F. (1990) *Science 250*, 646−651.
49. Eisenberg, D., and McLachlan, A. D. (1986) *Nature 319*, 199−203.

BI020486R